
STRUCTURAL SCIENCE
CRYSTAL ENGINEERING
MATERIALS

**Volume 78 (2022)**

**Supporting information for article:**

# Structure determination from unindexed powder data from scratch by a global optimization approach using pattern comparison based on cross-correlation functions

**Stefan Habermehl, Carina Schlesinger and Martin U. Schmidt**

Acta Crystallographica Section B
**Structural Science, Crystal Engineering and Materials**

# Electronic Supplementary Information (ESI) - Habermehl *et al.* (2022): Structure determination from unindexed powder data from scratch by a global optimization approach using pattern comparison based on cross-correlation functions

## S1. Powder diffraction details

In order to test and demonstrate the capabilities of the *FIDEL-GO* method, the application examples all started with problematic powder diffraction data. An overview of the XRPD measurements of the four samples is shown in Table S1. The samples of the quinacridone derivatives DFQ, DCQ and DCDHQ inherently suffer from small domain sizes. Only the diffraction measurement of DFQ can be regarded as a best-practice measurement for SDPD with standard laboratory equipment. The powder patterns of DCQ and DCDHQ are from routine measurements for phase identification. The test case for the known structure of CuCP was intentionally based on the example of a fast overview measurement.

**Table S1**
Details of the XRPD measurements in transmission mode with Cu $K\alpha_1$ radiation at room temperature on STOE STADI-P diffractometers with a curved Ge(111) monochromator and a linear position-sensitive detector.

| Sample | $2\theta$ range / ° | $2\theta$ stepsize / ° | Max. intensity / counts |
|---|---|---|---|
| DFQ | 2.00 - 79.99 | 0.01 | 94026 |
| DCQ | 3.00 - 33.98 | 0.02 | 3807 |
| DCDHQ | 3.00 - 33.98 | 0.02 | 6526 |
| CuCP | 2.00 - 59.99 | 0.01 | 708 |

## S2. Rietveld refinements details

### S2.1. Automatic Rietveld refinements (AR)

The automatic Rietveld refinements consist of a sequence of 7 *TOPAS* calls. The refinement sequence starts with two calls performing a Pawley fit (Pawley, 1981) to refine the background, described by 20 Chebyshev polynomial terms, the zero point error, the lattice parameters and a Gaussian and Lorentzian component convolution accounting for the crystallite size and strain broadening. The second run of the Pawley fit also includes the refinement of the peak width anisotropy, described by spherical harmonics of the $6^{th}$ order. The subsequent Rietveld refinement of the structure is performed in 5 steps. In the first step only the scaling factor is refined. In the second step the background is refined additionally. In the third step one isotropic displacement parameter is refined for all non-hydrogen atoms, while still refining the scale factor and the background. Hydrogen atoms are included with an isotropic displacement parameter of 1.2 times the value for non-hydrogen atoms. The automatic refinements of CuCP included two additional isotropic displacement parameters for copper and chlorine. In the fourth step the refinement of the atomic coordinates is added, using a high penalty weighting for the molecular geometry restraints. In the last RV step the same variables are refined using a less stricter penalty weighting.

### S2.2. User-controlled Rietveld refinements (UR)

The user-controlled refinements with *TOPAS* were always performed against the original (unsmoothed) powder data. They roughly followed the protocol described for the automatic refinement sequence or started from a certain stage of the automatic refinement sequence. At first, a Pawley refinement was carried out to refine the background, defined by 20 Chebyshev polynomial terms, the zero point error, the lattice parameters and the peak shape parameters, including peak asymmetry. The peak profile was described by the full axial divergence model using the method of Cheary & Coelho (1998). The parameters describing the background, the zero point and the peak shape were fixed at the beginning of the Rietveld refinement of the structural models. For DFQ and DCQ two isotropic displacement parameters for non-hydrogen atoms were refined, one for the halogen atom and one for carbon, nitrogen and oxygen atoms. The refinement of CuCP included two additional isotropic displacement parameters for copper and chlorine. It was always checked for preferred orientation. Preferred orientation was refined for DCQ, using the spherical harmonics description. In the investigation of the different structural models of DFQ (model A-D) and DCDHQ (models A1-C1) all models

for a given observed pattern were subjected to a strictly identical refinement procedure to ensure the comparability of the resulting structures. The final crystal structure (model B) of DFQ was further refined for the deposition in the CSD database. In the Rietveld refinement of CuCP the pyridine ring was restrained to be flat and C-C and C-H angles of the pyridine ring were restrained to 120°. At the end of the refinement of CuCP, the restraints for the Cu-Cl and Cu-N distances and all restraints on angles involving Cu atoms (Cl-Cu-N, Cu-N-C, etc.) were omitted, in order to search for possible Jahn-Teller-distortions of the octahedra.

## S3. Structure determination of 4,11-difluoro-quinacridone (DFQ)

The following tables supplement the description of the SDPD of DFQ in section 5.1 of the paper. They provide a detailed overview of the structure candidates processed and evaluated in the stages from the global optimization to the final Rietveld refinement: the results of the global optimization after the automatic reevaluation (stage RE2, Table S2), the automatic Rietveld refinements (stage AR, Table S3), the DFT-D geometry optimizations (stage DO, Table S4) and the user-controlled Rietveld refinements (stage UR, Table S5).

**Table S2**
DFQ: final results of the global optimization with *FIDEL-GO* (stage RE2).

| Rank | Model | Sp. gr. | $Z'$ | $R_{wp}$ / % | $S_{12}^0$ | $V/Z$ / Å$^3$/mol | $a$ / Å | $b$ / Å | $c$ / Å | $\alpha$ / ° | $\beta$ / ° | $\gamma$ / ° |
|---|---|---|---|---|---|---|---|---|---|---|---|---|
| 1 | A | $P2_1/c$ | 1 | 18.69 | 0.9891 | 358.87 | 13.685 | 3.763 | 28.794 | 90 | 104.50 | 90 |
| 2 | B | $P2_1/c$ | 0.5 | 20.02 | 0.9875 | 358.92 | 14.299 | 3.763 | 13.691 | 90 | 102.94 | 90 |
| 3 | | $P2_1/c$ | 1 | 20.00 | 0.9870 | 354.23 | 13.544 | 3.758 | 28.406 | 90 | 101.47 | 90 |
| 4 | | $P2_1/c$ | 1 | 23.21 | 0.9863 | 352.61 | 13.516 | 3.754 | 28.280 | 90 | 100.60 | 90 |
| 5 | | $P2_1/c$ | 1 | 25.25 | 0.9860 | 352.70 | 13.513 | 3.754 | 28.288 | 90 | 100.55 | 90 |
| 6 | | $P2_1/c$ | 1 | 25.49 | 0.9856 | 359.37 | 13.717 | 3.765 | 28.745 | 90 | 104.46 | 90 |
| 7 | | $P2_1/c$ | 0.5 | 20.97 | 0.9851 | 358.40 | 14.314 | 3.763 | 13.662 | 90 | 103.05 | 90 |
| 8 | C | $P\bar{1}$ | 0.5 | 22.55 | 0.9840 | 369.82 | 3.900 | 7.110 | 14.274 | 100.95 | 93.50 | 106.40 |
| 9 | | $P\bar{1}$ | 0.5 | 22.54 | 0.9839 | 369.53 | 3.896 | 7.111 | 14.264 | 100.79 | 93.47 | 106.47 |
| 10 | | $P\bar{1}$ | 0.5 | 25.96 | 0.9839 | 359.11 | 3.675 | 7.104 | 14.099 | 98.90 | 90.55 | 98.78 |
| 11 | | $P1$ | 1 | 22.78 | 0.9839 | 370.01 | 3.903 | 7.099 | 14.263 | 100.74 | 93.38 | 106.33 |
| 12 | | $P\bar{1}$ | 0.5 | 22.95 | 0.9838 | 370.32 | 3.904 | 7.101 | 14.264 | 100.72 | 93.29 | 106.34 |
| 13 | | $P\bar{1}$ | 0.5 | 23.18 | 0.9837 | 369.10 | 3.877 | 7.065 | 14.292 | 76.86 | 86.90 | 75.54 |
| 14 | | $P1$ | 1 | 23.05 | 0.9836 | 370.23 | 3.903 | 7.113 | 14.270 | 100.89 | 93.14 | 106.64 |
| 15 | | $P1$ | 1 | 22.43 | 0.9833 | 368.53 | 3.887 | 7.105 | 14.255 | 100.49 | 93.64 | 106.42 |
| 16 | | $P2_1/c$ | 1 | 25.43 | 0.9833 | 351.05 | 13.452 | 3.744 | 28.217 | 90 | 98.85 | 90 |
| ... | | | | | | | | | | | | |
| 28 | | $P\ 2_1/c$ | 0.5 | 19.85 | 0.9822 | 360.75 | 14.461 | 3.755 | 13.795 | 90 | 105.61 | 90 |
| ... | | | | | | | | | | | | |
| 34 | D | $P2_1/c$ | 1 | 29.88 | 0.9819 | 356.38 | 14.245 | 3.759 | 27.263 | 90 | 102.43 | 90 |
| ... | | | | | | | | | | | | |
| 47 | | $P2_1/c$ | 0.5 | 20.87 | 0.9804 | 355.81 | 14.484 | 3.753 | 13.595 | 90 | 105.65 | 90 |
| 61 | | $P\bar{1}$ | 0.5 | 24.15 | 0.9796 | 371.22 | 3.990 | 6.702 | 14.131 | 81.81 | 82.99 | 88.17 |

**Table S3**
DFQ: automatic Rietveld refinements (stage AR) of selected structural models from the global optimization with *FIDEL-GO*. Models with *Z*'=0.5 have been refined in corresponding subgroups with *Z*'=1 or in *P*1.

| Model | Sp. gr. | *Z* | $R_{exp}$ / % | $R_{wp}$ / % | $R_{wp}$' / % | *GoF* | *V*/*Z* / Å$^3$/mol | *a* / Å | *b* / Å | *c* / Å | $\alpha$ / ° | $\beta$ / ° | $\gamma$ / ° |
|---|---|---|---|---|---|---|---|---|---|---|---|---|---|
| B | $P1$ | 2 | 1.095 | 7.484 | 14.021 | 6.833 | 355.25 | 14.391 | 3.763 | 13.603 | 90 | 105.33 | 90 |
| | $P1$ | 2 | 1.095 | 8.149 | 14.740 | 7.440 | 356.53 | 14.199 | 3.766 | 13.655 | 90 | 102.44 | 90 |
| | $P2_1/c$ | 4 | 1.107 | 10.055 | 19.091 | 9.080 | 353.25 | 13.561 | 3.763 | 28.301 | 90 | 101.96 | 90 |
| | $P2_1/c$ | 4 | 1.107 | 10.516 | 19.092 | 9.497 | 352.35 | 13.521 | 3.761 | 28.232 | 90 | 100.95 | 90 |
| | $P2_1/c$ | 4 | 1.107 | 10.699 | 19.459 | 9.662 | 352.25 | 13.520 | 3.760 | 28.248 | 90 | 101.14 | 90 |
| A | $P2_1/c$ | 4 | 1.107 | 10.888 | 20.659 | 9.832 | 358.23 | 13.687 | 3.770 | 28.687 | 90 | 104.54 | 90 |
| | $P2_1/c$ | 4 | 1.107 | 11.595 | 21.526 | 10.471 | 351.39 | 13.467 | 3.763 | 28.121 | 90 | 99.44 | 90 |
| C | $P1$ | 1 | 1.107 | 11.966 | 22.419 | 10.808 | 367.71 | 3.896 | 7.043 | 14.201 | 102.26 | 86.80 | 105.06 |
| | $P2_1/c$ | 2 | 1.113 | 12.102 | 22.476 | 10.871 | 359.16 | 14.402 | 3.762 | 13.770 | 90 | 105.68 | 90 |
| D | $P2_1/c$ | 4 | 1.107 | 12.822 | 23.162 | 11.580 | 353.94 | 14.148 | 3.764 | 27.144 | 90 | 101.66 | 90 |
| | $P1$ | 1 | 1.107 | 12.407 | 23.520 | 11.207 | 358.19 | 3.674 | 7.099 | 14.062 | 98.83 | 91.38 | 98.318 |
| | $P1$ | 1 | 1.107 | 12.686 | 24.357 | 11.458 | 368.30 | 3.904 | 7.090 | 14.194 | 79.78 | 86.73 | 106.50 |
| | $P1$ | 1 | 1.107 | 12.995 | 24.722 | 11.738 | 368.74 | 3.905 | 7.097 | 14.209 | 100.57 | 93.65 | 106.33 |
| | $P2_1/c$ | 2 | 1.113 | 13.617 | 27.137 | 12.232 | 356.32 | 14.220 | 3.771 | 13.625 | 90 | 102.72 | 90 |
| | $P1$ | 1 | 1.107 | 14.263 | 28.678 | 12.883 | 368.42 | 3.897 | 7.096 | 14.216 | 79.47 | 86.13 | 106.12 |
| | $P\bar{1}$ | 1 | 1.113 | 16.846 | 29.905 | 15.135 | 372.27 | 4.013 | 6.696 | 14.074 | 82.23 | 96.42 | 92.12 |
| | $P1$ | 1 | 1.107 | 14.729 | 30.284 | 13.304 | 368.51 | 3.902 | 7.084 | 14.204 | 102.63 | 86.27 | 105.88 |
| | $P1$ | 1 | 1.107 | 17.055 | 34.873 | 15.405 | 366.21 | 3.885 | 7.110 | 14.405 | 103.70 | 93.78 | 106.79 |

**Table S4**
DFQ: DFT-D geometry optimizations of selected structural models. *CASTEP* calculations were performed with fixed cell dimensions at first and including the optimization of the lattice parameters in the second step. Energies given are relative to the lowest energy of all calculations.

| Structure candidate | | | Cell optimized | | Cell fixed | | | | | | | |
|---|---|---|---|---|---|---|---|---|---|---|---|---|
| Model | Sp. gr. | *Z*' | $\Delta E$ / kJ/mol | *V*/*Z* / Å$^3$/mol | $\Delta E$ / kJ/mol | *V* / Å$^3$/mol | *a* / Å | *b* / Å | *c* / Å | $\alpha$ / ° | $\beta$ / ° | $\gamma$ / ° |
| A | $P2_1/c$ | 1 | 0 | 336.7 | 5.18 | 358.87 | 13.685 | 3.763 | 28.794 | 90 | 104.50 | 90 |
| B | $P2_1/c$ | 0.5 | 0.54 | 337.2 | 5.57 | 358.92 | 14.299 | 3.763 | 13.691 | 90 | 102.94 | 90 |
| C | $P\bar{1}$ | 0.5 | 24.56 | 346.4 | 31.12 | 369.82 | 3.898 | 7.110 | 14.274 | 100.95 | 93.50 | 106.40 |
| D | $P2_1/c$ | 1 | 13.89 | 344.8 | 16.69 | 357.73 | 14.335 | 3.759 | 27.264 | 90 | 103.08 | 90 |
| | $P1$ | 1 | 25.12 | 344.5 | 31.60 | 369.53 | 3.896 | 7.111 | 14.264 | 100.79 | 86.53 | 106.47 |

**Table S5**
DFQ: user-controlled Rietveld refinements of selected structural models (stage UR) under strictly identical conditions and final refinement of the submitted structure (model B). Molecular geometry restraints were derived from DFT-D calculation.

| Model | Sp. gr. | *Z*' | $R_{exp}$ / % | $R_{wp}$ / % | $R_{wp}$' / % | *GoF* | *V*/*Z* / Å$^3$/mol | *a* / Å | *b* / Å | *c* / Å | $\alpha$ / ° | $\beta$ / ° | $\gamma$ / ° |
|---|---|---|---|---|---|---|---|---|---|---|---|---|---|
| A | $P2_1/c$ | 1 | 1.276 | 5.160 | 9.018 | 4.045 | 358.54 | 13.696 | 3.768 | 28.789 | 90 | 105.16 | 90 |
| | $P\,2_1/c$ | 1 | 1.276 | 6.442 | 11.581 | 5.050 | 354.47 | 13.589 | 3.763 | 28.346 | 90 | 101.97 | 90 |
| B | $P2_1/c$ | 0.5 | 1.280 | 6.759 | 12.249 | 5.279 | 358.33 | 14.217 | 3.768 | 13.704 | 90 | 102.50 | 90 |
| | $P\,2_1/c$ | 0.5 | 1.280 | 7.486 | 14.075 | 5.847 | 357.46 | 14.201 | 3.767 | 13.682 | 90 | 102.37 | 90 |
| D | $P2_1/c$ | 1 | 1.276 | 8.569 | 14.796 | 6.718 | 359.62 | 14.335 | 3.773 | 27.374 | 90 | 103.69 | 90 |
| C | $P\bar{1}$ | 0.5 | 1.280 | 9.946 | 17.679 | 7.770 | 361.44 | 3.885 | 7.033 | 14.101 | 102.71 | 86.08 | 105.94 |
| B final | $P2_1/c$ | 0.5 | 1.466 | 6.452 | 14.425 | 4.402 | 359.08 | 14.217 | 3.768 | 13.721 | 90 | 102.30 | 90 |

## S4. Structure determination of 2,9-dichloro-quinacridone (DCQ)

The SDPD of DCQ by global optimization (section 5.2.1 of the paper) is complemented by an overview of the top ranking primary results of the global optimizations in all investigated crystal symmetries (stage RE1, Table S6). The crystal structure of the best candidate from the global optimization is compared to the corresponding crystal structure after the DFT-D calculation in Fig. S1.

For the SDPD of DCQ by screening of CSP results (section 5.2.1 of the paper) an overview of the crystal structure prediction results is provided in Table S7.

**Table S6**
DCQ: primary results of the global optimization with *FIDEL-GO* (stage RE1). Best structure of each crystal symmetry.

| Sp. gr. | $Z$ | $S^0_{12,bc}$ | $V/Z$ / Å$^3$/mol | $a$ / Å | $b$ / Å | $c$ / Å | $\alpha$ / ° | $\beta$ / ° | $\gamma$ / ° |
|---|---|---|---|---|---|---|---|---|---|
| $P1$ | 1 | 0.9186 | 389.58 | 3.797 | 6.521 | 16.131 | 94.96 | 91.14 | 101.59 |
| $P2_12_12_1$ | 4 | 0.9176 | 389.94 | 3.721 | 6.530 | 64.184 | 90 | 90 | 90 |
| $P\bar{1}$ | 1 | 0.9165 | 388.45 | 3.790 | 6.507 | 16.135 | 94.70 | 91.52 | 101.32 |
| $P2_1/c$ | 4 | 0.8977 | 384.74 | 16.051 | 7.612 | 12.628 | 90 | 94.10 | 90 |
| $P2_1$ | 2 | 0.8944 | 341.12 | 4.228 | 10.148 | 15.926 | 90 | 93.32 | 90 |
| $P2_1/c$ | 2 | 0.8862 | 404.96 | 3.653 | 6.951 | 32.250 | 90 | 98.48 | 90 |
| $C2/c$ | 4 | 0.8747 | 337.61 | 11.698 | 3.614 | 32.219 | 90 | 97.57 | 90 |
| $C2/m$ | 2 | 0.8581 | 353.83 | 6.891 | 6.430 | 16.061 | 90 | 96.07 | 90 |
| $Pbca$ | 4 | 0.8272 | 352.02 | 6.426 | 6.880 | 31.847 | 90 | 90 | 90 |

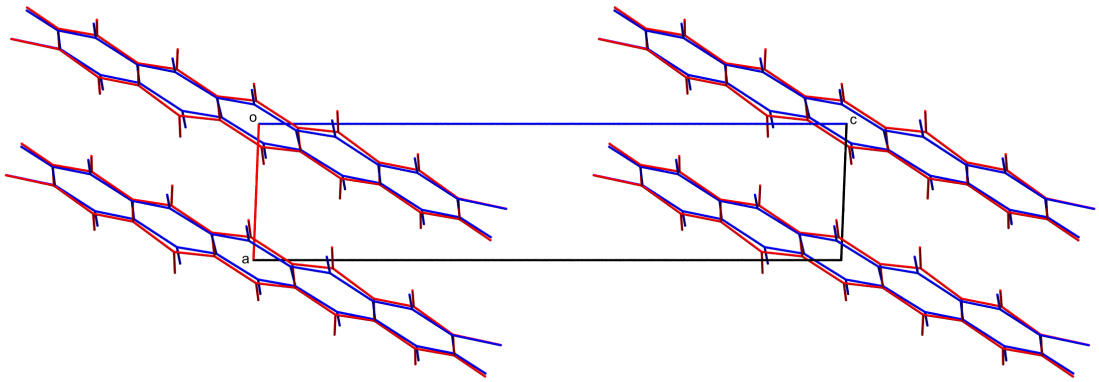


**Figure S1**
DCQ: structure overlay of the best candidate from the global optimization before (blue) and after (red) the DFT-D geometry optimization with fixed cell, view along [010].

**Table S7**
DCQ: crystal structure prediction by lattice energy minimization with *CRYSCA*. Lowest energy structure in each crystal symmetry, ranked by energy relative to the lowest energy of all calculations.

| Sp. gr. | $Z$ | $Z'$ | Site symm. | CSP results | $\Delta E$ / kJ/mol | $V/Z$ / Å$^3$/mol | $a$ / Å | $b$ / Å | $c$ / Å | $\alpha$ / ° | $\beta$ / ° | $\gamma$ / ° |
|---|---|---|---|---|---|---|---|---|---|---|---|---|
| $P1$ | 1 | 1 | 1 | 500 | 0 | 408.35 | 4.156 | 6.879 | 14.640 | 82.06 | 86.37 | 80.35 |
| $P\bar{1}$ | 1 | 0.5 | $\bar{1}$ | 118 | 4.44 | 410.59 | 3.778 | 7.033 | 15.617 | 91.24 | 91.12 | 98.14 |
| $P\bar{1}$ | 2 | 1 | 1 | 157 | 6.88 | 420.43 | 7.428 | 8.483 | 14.684 | 90.87 | 100.28 | 111.97 |
| $P2_1/c$ | 2 | 0.5 | $\bar{1}$ | 585 | 7.81 | 405.90 | 7.337 | 17.347 | 7.196 | 90 | 117.58 | 90 |
| $P2_1$ | 2 | 1 | 1 | 318 | 8.85 | 419.03 | 7.421 | 6.700 | 16.856 | 90 | 89.60 | 90 |
| $Pbca$ | 4 | 0.5 | $\bar{1}$ | 244 | 11.11 | 414.78 | 7.466 | 6.497 | 34.202 | 90 | 90 | 90 |
| $Pbca$ | 8 | 1 | 1 | 112 | 11.38 | 408.64 | 7.454 | 6.695 | 65.511 | 90 | 90 | 90 |
| $P2_1/c$ | 4 | 1 | 1 | 128 | 12.61 | 412.17 | 33.370 | 7.403 | 6.765 | 90 | 99.43 | 90 |
| $P2/c$ | 2 | 0.5 | $\bar{1}$ | 1190 | 13.05 | 415.20 | 6.361 | 3.899 | 37.649 | 90 | 117.21 | 90 |
| $P2_12_12_1$ | 4 | 1 | 1 | 146 | 16.69 | 428.26 | 7.457 | 31.898 | 7.202 | 90 | 90 | 90 |
| $P2/c$ | 4 | 1 | 1 | 179 | 21.20 | 459.22 | 43.822 | 7.513 | 6.917 | 90 | 126.23 | 90 |

## S5. Structure determination of 2,9-dichloro-6,13-dihydro-quinacridone (DCDHQ)

The crystal symmetries under investigation in the global optimization runs for DCDHQ (section 5.3 of the paper) are documented in Table S8. An overview of the top ranking primary results of the global optimizations in all crystal symmetries (stage RE1) is shown in Table S9. Table S10 lists the results of the automatic Rietveld refinements (stage AR) and the results of the DFT-D geometry optimizations (stage DO) are documented in Table S11.

The crystal structures and the corresponding Rietveld plots of the structural models B1Z1, B1, A3 and C1 are shown in Fig. S2. A detailed discussion of the structure candidates is provided in §S5.2.

**Table S8**
DCDHQ: selection of the crystal symmetries for the global optimization. For setups of planar molecules (point group $C_{2h}$) with $Z'$=0.5 the inversion center of the molecule has been positioned at the crystallographic inversion center using a dummy atom.

| Crystal system | Space group | $Z$ | $Z'$ | Site symm. | Intramol. DOFs | Fitted parameters |
|---|---|---|---|---|---|---|
| Triclinic | $P\bar{1}$ | 1 | 0.5 | $\bar{1}$ | 0 | 9 |
| | | 2 | 1 | 1 | 2 | 14 |
| Monoclinic | $P2_1$ | 2 | 1 | 1 | 2 | 11 |
| | $C2/c$ | 8 | 1 | 1 | 2 | 12 |
| | $P2_1/c$ | 2 | 0.5 | $\bar{1}$ | 0 | 7 |
| | | 4 | 1 | 1 | 2 | 12 |
| Orthorhombic | $P2_12_12_1$ | 4 | 1 | 1 | 2 | 11 |
| | $Pbca$ | 8 | 1 | 1 | 2 | 11 |
| | $Pna2_1$ | 4 | 1 | 1 | 2 | 11 |

**Table S9**
DCDHQ: primary results of the global optimization with*FIDEL-GO* (stage RE1). Best structure of each crystal symmetry.

| Sp. gr. | $Z$ | opt. runs | $S^0_{12,bc}$ | $V/Z$ / Å$^3$/mol | $a$ / Å | $b$ / Å | $c$ / Å | $\alpha$ / ° | $\beta$ / ° | $\gamma$ / ° |
|---|---|---|---|---|---|---|---|---|---|---|
| $P\bar{1}$ | 2 | 4 | 0.9547 | 417.69 | 4.118 | 12.973 | 16.657 | 70.09 | 88.68 | 86.93 |
| $P2_1/c$ | 2 | 4 | 0.9528 | 417.56 | 6.487 | 4.097 | 31.475 | 90 | 93.35 | 90 |
| $P\bar{1}$ | 1 | 4 | 0.9521 | 378.80 | 3.743 | 6.601 | 15.656 | 86.95 | 89.41 | 78.74 |
| $C2/c$ | 8 | 4 | 0.9475 | 285.99 | 12.943 | 5.645 | 31.346 | 90 | 92.54 | 90 |
| $P2_1/c$ | 1 | 4 | 0.9422 | 390.68 | 6.622 | 62.731 | 3.769 | 90 | 93.58 | 90 |
| $P2_1$ | 2 | 2 | 0.9330 | 459.39 | 4.135 | 31.274 | 7.189 | 90 | 98.74 | 90 |
| $Pbca$ | 8 | 1 | 0.9284 | 379.76 | 14.205 | 31.327 | 6.827 | 90 | 90 | 90 |
| $P2_12_12_1$ | 4 | 2 | 0.9261 | 419.09 | 7.104 | 7.527 | 31.350 | 90 | 90 | 90 |
| $Pna2_1$ | 4 | 2 | 0.9234 | 421.34 | 62.767 | 3.777 | 7.110 | 90 | 90 | 90 |

**Table S10**
DCDHQ: automatic Rietveld refinements (stage AR) of selected structural models from the global optimization by *FIDEL-GO*, ranked by $R_{wp}$'. Models with $Z'$=0.5 have been refined in corresponding subgroups with $Z'$=1.

| Model | Sp. gr. | $Z$ | $R_{exp}$ / % | $R_{wp}$ / % | $R_{wp}$' / % | *GoF* | $V/Z$ / Å$^3$/mol | $a$ / Å | $b$ / Å | $c$ / Å | $\alpha$ / ° | $\beta$ / ° | $\gamma$ / ° |
|---|---|---|---|---|---|---|---|---|---|---|---|---|---|
| A1 | $P1$ | 1 | 2.988 | 7.781 | 20.386 | 2.604 | 382.12 | 3.775 | 6.577 | 15.643 | 87.33 | 89.02 | 99.87 |
| A2 | $P1$ | 1 | 2.988 | 7.846 | 20.388 | 2.626 | 382.38 | 3.778 | 6.583 | 15.642 | 92.66 | 89.05 | 79.80 |
| B1 | $P\bar{1}$ | 2 | 2.988 | 8.637 | 21.282 | 2.891 | 414.44 | 16.634 | 4.095 | 13.976 | 111.94 | 107.54 | 92.42 |
| | $P1$ | 1 | 2.988 | 7.919 | 21.318 | 2.650 | 394.48 | 3.899 | 6.729 | 15.638 | 87.13 | 89.62 | 74.32 |
| C1 | $P2_1$ | 2 | 2.990 | 8.268 | 21.430 | 2.765 | 417.07 | 6.480 | 4.118 | 34.471 | 90 | 114.93 | 90 |
| A3 | $P1$ | 1 | 2.988 | 7.869 | 21.659 | 2.633 | 416.23 | 4.140 | 6.553 | 15.571 | 92.89 | 89.04 | 99.32 |
| A4 | $P1$ | 1 | 2.988 | 8.287 | 21.930 | 2.773 | 375.06 | 3.710 | 6.587 | 16.153 | 84.68 | 75.34 | 79.56 |
| | $P1$ | 1 | 2.988 | 8.655 | 21.964 | 2.897 | 378.09 | 3.736 | 6.653 | 15.650 | 93.24 | 88.10 | 103.13 |
| | $P1$ | 1 | 2.988 | 8.314 | 22.144 | 2.782 | 428.40 | 4.236 | 6.493 | 15.689 | 86.83 | 94.83 | 93.92 |
| | $P1$ | 1 | 2.988 | 8.415 | 22.679 | 2.816 | 426.14 | 4.205 | 6.501 | 15.667 | 86.91 | 87.56 | 85.67 |
| B2 | $P\bar{1}$ | 2 | 2.988 | 8.875 | 23.338 | 2.970 | 413.34 | 4.082 | 13.422 | 16.637 | 71.26 | 91.95 | 74.96 |
| A5 | $P1$ | 1 | 2.988 | 9.060 | 24.889 | 3.032 | 410.59 | 7.689 | 4.054 | 15.738 | 96.09 | 89.13 | 122.57 |
| | $P1$ | 1 | 2.988 | 9.006 | 25.071 | 3.014 | 416.16 | 4.111 | 6.479 | 15.741 | 92.95 | 83.69 | 90.97 |
| | $P1$ | 1 | 2.988 | 9.278 | 25.701 | 3.105 | 436.99 | 4.320 | 6.485 | 15.716 | 87.49 | 95.73 | 87.08 |
| | $P1$ | 1 | 2.988 | 9.475 | 26.155 | 3.171 | 418.02 | 4.126 | 6.480 | 15.737 | 87.04 | 95.80 | 90.93 |
| | $P\bar{1}$ | 2 | 2.988 | 11.785 | 29.670 | 3.944 | 368.30 | 6.958 | 7.006 | 17.195 | 72.02 | 67.97 | 79.24 |

**Table S11**
DCDHQ: DFT-D geometry optimizations of selected structural models (stage DO). *CASTEP* calculations were performed with fixed cell dimensions (a) at first and including the optimization of the lattice parameters (b) in the second step. Models are ranked by molar energies for each step. Energy values given are relative to the lowest energy of all calculations.

| Model | Sp. gr. | $Z$ | $\Delta E$ / kJ/mol | $V/Z$ / Å$^3$/mol | $a$ / Å | $b$ / Å | $c$ / Å | $\alpha$ / ° | $\beta$ / ° | $\gamma$ / ° |
|---|---|---|---|---|---|---|---|---|---|---|
| a) Cell fixed: | | | | | | | | | | |
| B1 | $P\bar{1}$ | 2 | 21.71 | 414.45 | 4.062 | 13.020 | 16.729 | 109.30 | 92.95 | 94.92 |
| A2 | $P\bar{1}$ | 1 | 27.96 | 381.80 | 3.770 | 6.601 | 15.633 | 92.73 | 90.36 | 100.73 |
| A1 | $P\bar{1}$ | 1 | 28.62 | 378.89 | 3.747 | 6.572 | 15.635 | 92.79 | 90.29 | 99.81 |
| A3 | $P\bar{1}$ | 1 | 33.47 | 420.87 | 4.152 | 6.577 | 15.668 | 86.56 | 88.45 | 80.25 |
| A5 | $P\bar{1}$ | 1 | 35.13 | 410.27 | 4.037 | 6.483 | 15.800 | 93.04 | 96.42 | 91.02 |
| B2 | $P\bar{1}$ | 2 | 36.03 | 419.14 | 4.118 | 13.418 | 16.670 | 71.37 | 91.32 | 75.20 |
| C1 | $P2_1/c$ | 2 | 40.47 | 417.56 | 6.487 | 4.097 | 31.475 | 90 | 93.35 | 90 |
| A4 | $P\bar{1}$ | 1 | 142.73 | 374.56 | 3.702 | 6.586 | 16.179 | 84.57 | 75.22 | 79.49 |
| b) Cell optimized: | | | | | | | | | | |
| A3 | $P\bar{1}$ | 1 | 0 | 367.92 | 3.697 | 6.596 | 15.563 | 92.11 | 88.94 | 104.00 |
| B1 | $P\bar{1}$ | 2 | 1.07 | 366.61 | 3.683 | 12.777 | 16.680 | 110.15 | 93.98 | 92.40 |
| A5 | $P\bar{1}$ | 1 | 1.60 | 368.79 | 3.690 | 6.620 | 15.594 | 87.85 | 88.23 | 75.70 |
| A2 | $P\bar{1}$ | 1 | 10.21 | 367.29 | 3.626 | 6.626 | 15.727 | 87.36 | 88.729 | 103.21 |
| A1 | $P\bar{1}$ | 1 | 10.38 | 367.31 | 3.625 | 6.616 | 15.718 | 92.53 | 88.592 | 77.40 |
| A4 | $P\bar{1}$ | 1 | 12.68 | 374.30 | 3.639 | 6.697 | 17.153 | 100.95 | 70.42 | 107.24 |
| C1 | $P2_1/c$ | 2 | 17.19 | 378.19 | 6.779 | 3.650 | 30.572 | 90 | 90.40 | 90 |
| B2 | $P\bar{1}$ | 2 | 19.41 | 383.76 | 4.5708 | 13.240 | 14.585 | 67.07 | 89.65 | 72.19 |

Model B1Z1

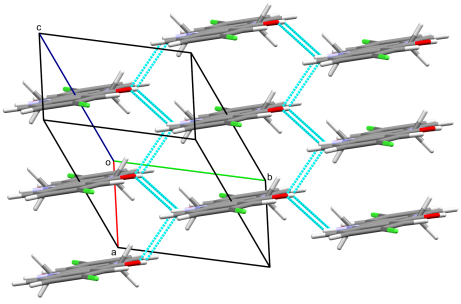


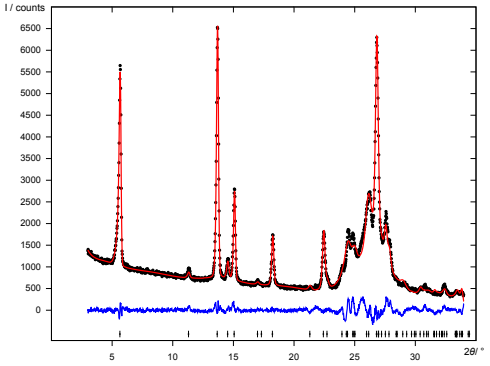


Model B1

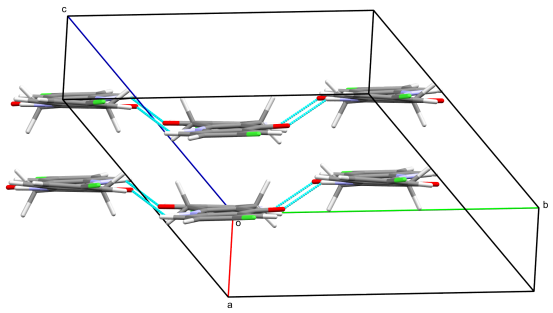


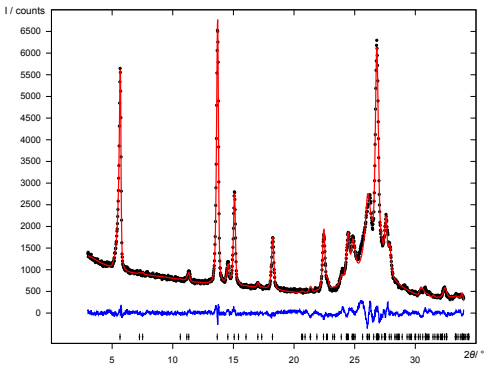


Model A3

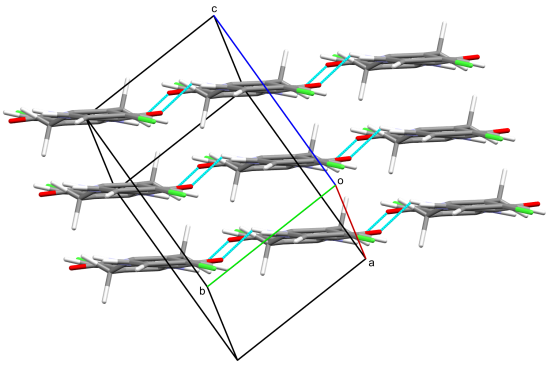


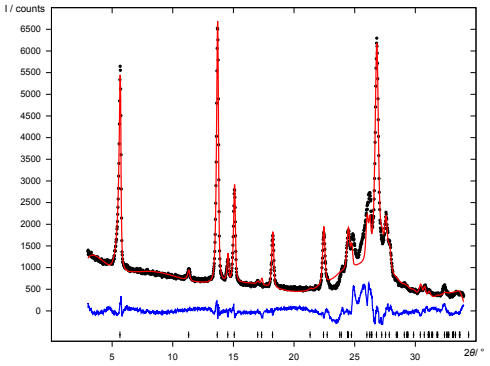


Model C1

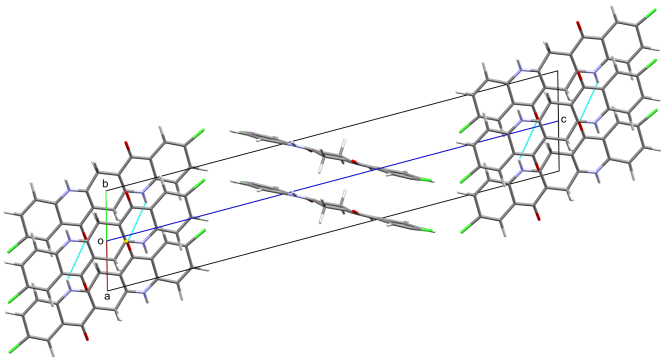


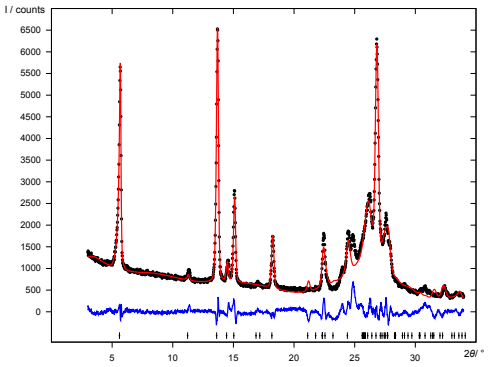


**Figure S2**
DCDHQ: crystal structures and Rietveld plots of the structural models B1Z1, B1, A3 and C1.

## S5.1. On the molecular conformation of DCDHQ

Before the *FIDEL* calculations, we investigated the possible molecular conformations of DCDHQ by searches in the Cambridge Structural Database (CSD). The first search with the fragment F1 (Fig. S3) did not yield any crystal structure containing this fragment. The compounds F2 (Fig. S3) with methyl, ethyl, butyl or octyl groups are all planar (CSD refcodes TUCBOL, TUCBUR, TUCCAY, TUICCEC, PILLAY) (Huang *et al.*, 2018).

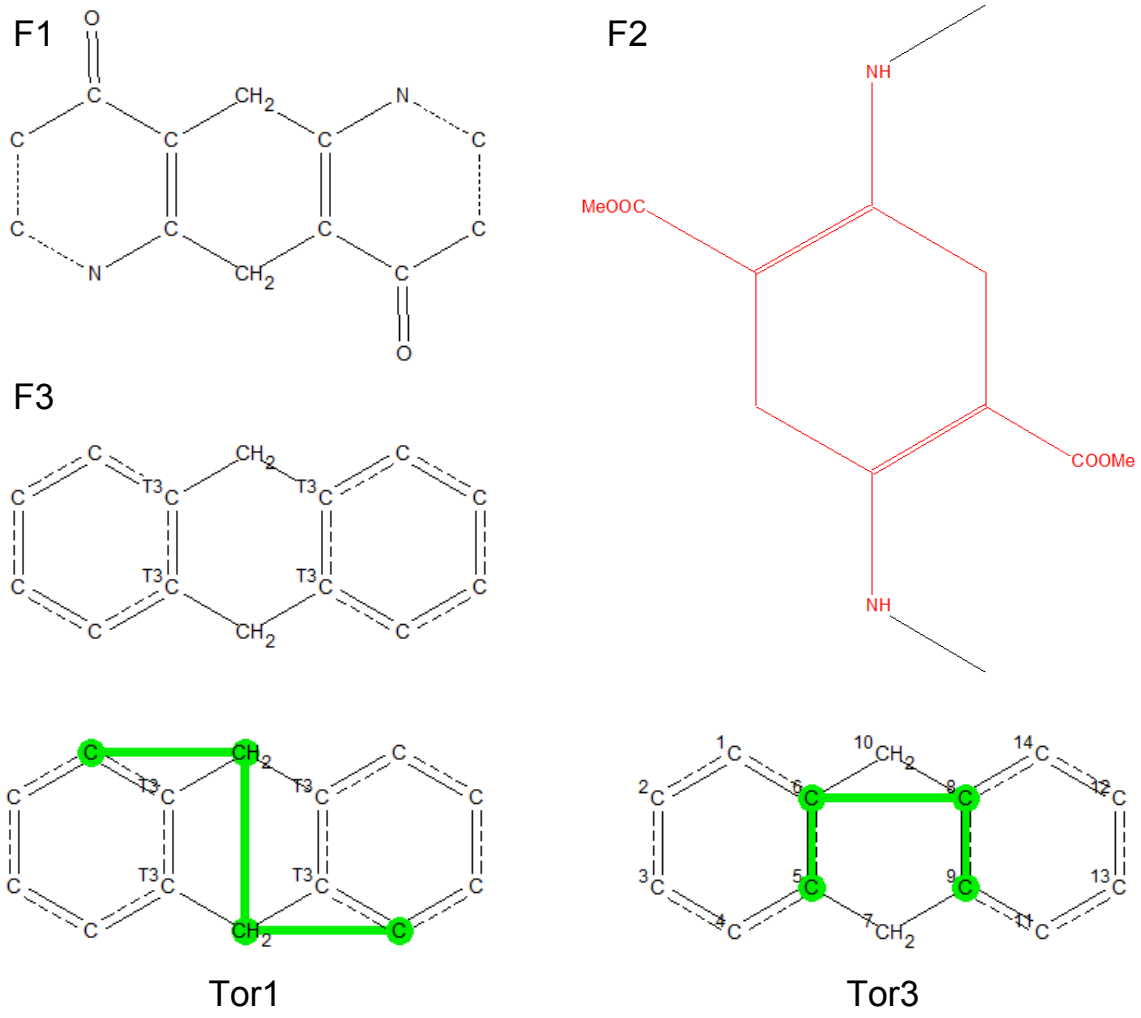


**Figure S3**
DCDHQ conformation, CSD searches: Definitions of search fragments F1, F2 and F3, and torsion angles Tor1 and Tor3. T3 denotes an atom with three bonds.

The next search was carried out with the fragment F3 (Fig. S3). Two torsion angles Tor1 and Tor3 (Fig. S3) were defined, that correspond to a tilting and a twisting of the molecule. The majority of these compounds is not planar. The distribution of the torsion angle Tor1 is shown in Fig. S4a.

9,10-Dihydro-anthracene itself (CSD refcode DITBOX01) has in the solid state a dihedral angle between the two benzene planes of 36.5° (corresponding to a torsion angle Tor1 of 143.5°). In contrast, the distribution of Tor3 is quite narrow (Fig. S4b).

These data show, that DCDHQ may be planar or tilted. In the *FIDEL* calculations, we allowed the molecule to tilt and to twist.

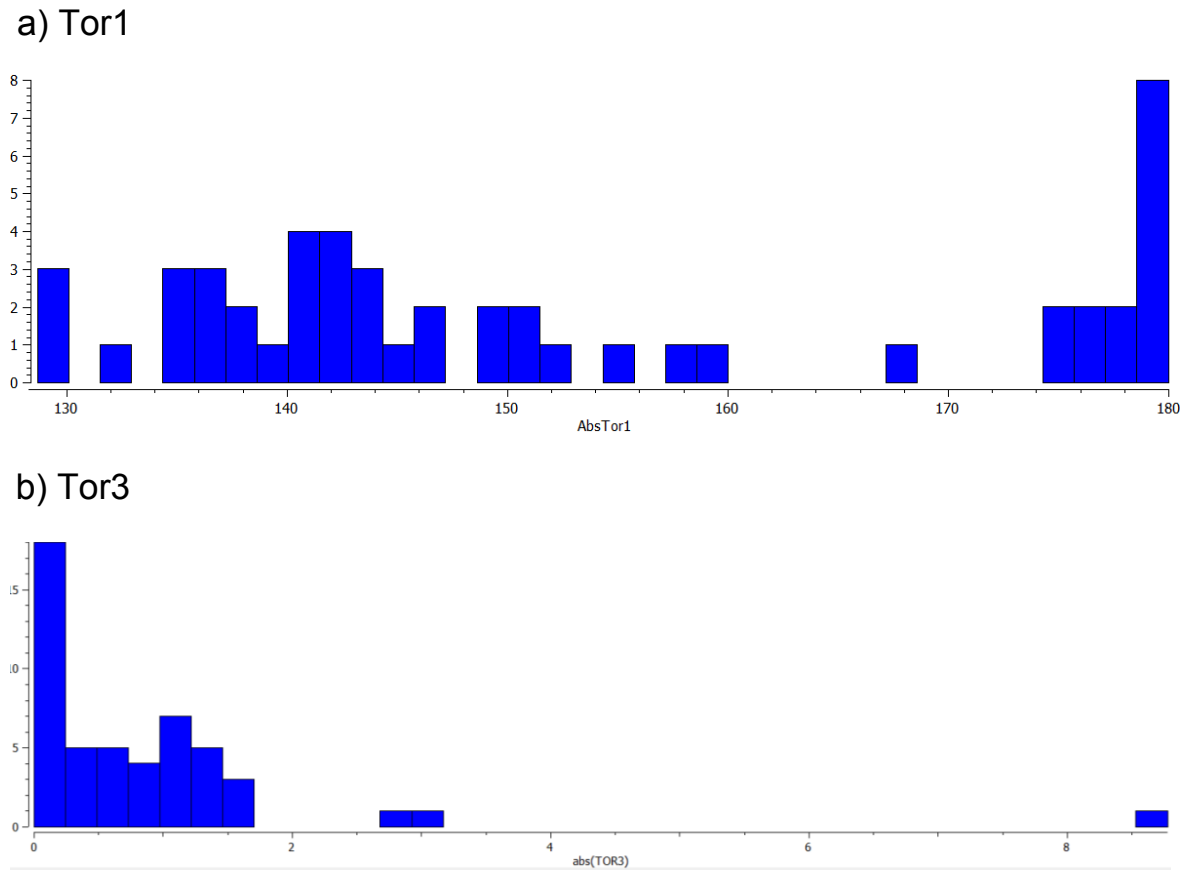


**Figure S4**
DCDHQ conformation, CSD search for fragment F3: Distribution of torsion angles (a) Tor1 and (b) Tor3.

### S5.2. Detailed discussion on DCDHQ

The results of the user-controlled Rietveld refinements of the models A1, A3, A4, B1 and C1 are listed in Table 8 in the paper. The structure refinements all suffer to some degree from considerable drawbacks in terms of the difference curve, unusual deviations in the molecular geometry or relatively high errors of the refined parameters. The refinement of the model B1 ($Z$=2) led to a best possible result of the attempt to determine the structure from the "real life" powder pattern under investigation. This is supported by the best of all difference curves achieved, the low energies of the geometry optimizations of B1, a quite typical molar volume and the plausibility of the packing motive of the molecules (Fig. S2).

However, there is by no means sufficient evidence to prove the existence of a wavy chain structure in $P\bar{1}$ with $Z$=2. On the contrary, the most likely assumption on the crystal structure of DCDHQ that can be drawn from this investigation is, that the dihydro-compound crystallizes in $P\bar{1}$ ($Z'$=0.5), just like other triclinic structures of un- or 2,9-disubstituted quinacridones, in particular the $\alpha$- and $\gamma$-phase of DCQ (see section 5.2 in the paper). This assumption is heavily supported by the DFT-D calculations (Table S11), that clearly show, that there is no significant advantage of the crystal symmetry with $Z'$=1 and that a packing in $P\bar{1}$ ($Z'$=0.5) is practically equivalent in terms of lattice energy and molar volume. In the resulting structure of the refinement of B1 there is a tilt of about 7° between two fairly planar halves of the molecule. Cell transformation of the structure with $b'=a/2+b/2$ led to a structural model with two of these tilted molecules to both sides of a plane that would represent the position of a fully planar molecule in $P\bar{1}$ ($Z'$=0.5), with the terminal chorine atoms at a mean distance of 0.14 Å and the $sp^3$-carbons in the central ring at a mean distance of 0.48 Å from the plane. While none of the quantum mechanical calculations gives rise to the expectation of a significant deviation from full planarity of the molecule, there may exist a non-neglectable tendency towards a slight tilt or twist of the molecules in the solid phase, leading to deviations from the perfect symmetry $P\bar{1}$ ($Z'$=0.5), e.g. a structure exhibiting orientational disorder. Two structure candidates selected for the user-controlled Rietveld refinement started from the primary results of the top ranking candidates of the global optimization by *FIDEL-GO* in $P2_1/c$ ($Z'$=0.5, model C1) and $P\bar{1}$ ($Z'$=0.5, model A4) (see Table 7 in the paper).

The packing index (PI) of the structural models, calculated by *PLATON* (Spek, 2009), has also been evaluated and compared to similar compounds. The PI of the structural models B1 and A3 converged to a value of about 80% on full DFT-D geometry optimization, while the PI of their Rietveld refinement results is at about 75%. This is in perfect agreement with known structures of

unsubstituted and disubstituted quinacridones, where the corresponding PI values span from 72.4% for unsubstituted $\gamma$-quinacridone up to 82.4% for a fully geometry optimized structure of 2,9-dimethyl-quinacridone. The structure candidate C1 in $P2_1/c$ ($Z$'=0.5) can be regarded as very unlikely, considering that all of its variants under investigation exhibited PI values of about 70-71%, more than 1% below the PI of any known crystal structure found so far for the compound class. The highest PI values of structural models, that were at least roughly considerable in the light of the DFT-D calculations and the Rietveld refinements for the room temperature structure, were found for three models in $P\bar{1}$ ($Z$'=0.5, models A1, A2 and A4). Their PI in the range 76.8-77.4% indicates a low likelihood of being a reasonable and correct representation of the crystal structure of DCDHQ, also taking into account the PI value 76.6% of the $\alpha$-phase of DCQ (section 5.2 in the paper).

The powder pattern of DCDHQ came from a routine measurement of an intermediate in the industrial synthesis of DCQ. The sample had not been subjected to recrystallization or other attempts to increase its purity and crystallinity before the measurement. Accordingly, the experimental data probably suffer at least to some degree from various conditions, that inevitably limit the possibility of a fully satisfactory structure determination, such as chemical impurities, the minor presence of other phases and disturbances of order in the crystalline domains of the sample. Although the attempted SDPD was not able to yield a fully satisfactory and decisive result, it shows very well both the capabilities and the limitations of the global optimization approach of *FIDEL-GO* and its general framework for SDPD.

Finally, the structure B1 ($P\bar{1}$, $Z$=2) was transformed to $P\bar{1}$, $Z$=1 by $a'=a$, $b'=a/2+b/2$, $c'=a/2+b/2+c$ (model B1Z1). The subsequent user-controlled Rietveld refinement of B1Z1 was carried out in a different way than that of A1, A3, A4, B1 and C1 (15 instead of 10 background parameters; peak-width anisotropy described by spherical harmonics of the $2^{nd}$ instead of the $4^{th}$ order; $B_{iso}$(C, N, O) fixed to 3.0 and $B_{iso}$(Cl, H) fixed to 3.6; etc.). The resulting structure (Fig. S2) differs from structure A3 by a rotation of the molecules around their long axis, leading to a different hydrogen bond system: whereas A3 contains chains with steps, the molecules in B1Z1 exhibit bifurcated hydrogen bonds to four neighbouring molecules. All N···O distances are equal (3.32 Å). Such a packing has not been observed for any other quinacridone derivative. Due to the limited information content of the powder data, it remains unclear, if the structure actually exhibits these bifurcated hydrogen bonds or consists of chains with steps, as found in several other quinacridone derivatives, or even of wavy chains, as shown in Fig. S2.

## S6. Structure determination of dichloro-bis(pyridine-N)-copper(II) (CuCP)

The crystal symmetries under investigation in the global optimization of CuCP (section 5.4 of the paper) are documented in Table S12. An overview of the top ranking primary results of the global optimizations in all crystal symmetries (stage RE1) is shown in Table S13. The automatic Rietveld refinements (stage AR) are documented in Table S14 and the DFT-D geometry optimizations (stage DO) in Table S15. The excellent agreement of the published single crystal structure and the crystal structure from the SDPD with *FIDEL-GO* is illustrated by the structure overlay in Fig. S5.

**Table S12**
CuCP: selection of the crystal symmetries for the global optimization. For setups with *Z'*=0.5 the metal atom has been fixed at the crystallographic inversion center.

| Crystal system | Space group | *Z* | *Z'* | Site symm. | Internal DOFs | Fitted parameters |
|---|---|---|---|---|---|---|
| Triclinic | $P\bar{1}$ | 1 | 0.5 | $\bar{1}$ | 4 | 13 |
| | | 2 | 1 | 1 | 10 | 19 |
| Monoclinic | $P2_1$ | 2 | 1 | 1 | 10 | 19 |
| | $C2/c$ | 4 | 0.5 | $\bar{1}$ | 4 | 11 |
| | | 8 | 1 | 1 | 10 | 20 |
| | $P2_1/c$ | 2 | 0.5 | $\bar{1}$ | 4 | 11 |
| | | 4 | 1 | 1 | 10 | 20 |
| Orthorhombic | $P2_12_12_1$ | 4 | 1 | 1 | 10 | 19 |
| | $Pbca$ | 4 | 0.5 | $\bar{1}$ | 4 | 10 |

**Table S13**
CuCP: primary results of the global optimization (stage RE1). Best structure of each crystal symmetry.

| Sp. gr. | *Z* | $S^0_{12,bc}$ | *V*/*Z* / Å$^3$/mol | *a* / Å | *b* / Å | *c* / Å | $\alpha$ / ° | $\beta$ / ° | $\gamma$ / ° |
|---|---|---|---|---|---|---|---|---|---|
| $P2_1/c$ | 2 | 0.9728 | 281.28 | 3.855 | 8.584 | 17.308 | 90 | 100.84 | 90 |
| $P2_1/c$ | 4 | 0.9662 | 282.29 | 7.724 | 8.589 | 17.338 | 90 | 100.99 | 90 |
| $P2_1$ | 2 | 0.9648 | 282.03 | 3.861 | 8.585 | 17.024 | 90 | 91.84 | 90 |
| $C2/c$ | 8 | 0.9536 | 305.51 | 11.742 | 12.421 | 16.766 | 90 | 91.78 | 90 |
| $P\bar{1}$ | 1 | 0.9482 | 277.35 | 3.799 | 8.579 | 9.519 | 116.48 | 90.78 | 92.09 |
| $C2/c$ | 4 | 0.9414 | 313.82 | 9.485 | 17.016 | 8.593 | 90 | 115.16 | 90 |
| $P\bar{1}$ | 2 | 0.9394 | 309.79 | 8.324 | 8.974 | 9.770 | 112.81 | 102.04 | 102.85 |
| $P2_12_12_1$ | 4 | 0.9232 | 307.76 | 8.418 | 8.604 | 16.998 | 90 | 90 | 90 |
| $Pbca$ | 4 | 0.8976 | 290.44 | 16.935 | 3.992 | 17.186 | 90 | 90 | 90 |

**Table S14**
CuCP: automatic Rietveld refinements (stage AR) in $P2_1$, *Z*=2 vs. smoothed powder pattern.

| Model | $R_{exp}$ / % | $R_{wp}$ / % | $R_{wp}$' / % | *GoF* | *V*/*Z* / Å$^3$/mol | *a* / Å | *b* / Å | *c* / Å | $\beta$ / ° |
|---|---|---|---|---|---|---|---|---|---|
| A1 | 2.372 | 7.935 | 8.866 | 3.346 | 281.55 | 3.862 | 8.580 | 17.308 | 100.91 |
| B1 | 2.372 | 8.939 | 10.012 | 3.769 | 281.58 | 3.862 | 8.579 | 17.309 | 100.90 |
| B2 | 2.372 | 9.765 | 10.988 | 4.118 | 281.57 | 3.862 | 8.579 | 17.309 | 100.90 |

**Table S15**
CuCP: DFT-D geometry optimizations (stage DO) of selected structural models in $P2_1/c$, *Z*=2. *CASTEP* calculations were performed with fixed cell dimensions at first and including the optimization of the lattice parameters in the second step. Energies shown are relative to the lowest energy of all calculations.

| Model | Cell optimized | | Cell fixed | | | | | |
|---|---|---|---|---|---|---|---|---|
| | $\Delta E$ / kJ/mol | *V*/*Z* / Å$^3$/mol | $\Delta E$ / kJ/mol | *V*/*Z* / Å$^3$/mol | *a* / Å | *b* / Å | *c* / Å | $\beta$ / ° |
| A1 | 0 | 540.68 | 2.43 | 563.11 | 3.862 | 8.580 | 17.308 | 100.91 |
| B1 | 0.24 | 539.02 | 3.64 | 564.72 | 3.864 | 8.592 | 17.320 | 100.86 |
| B2 | not done | not done | 2.47 | 563.15 | 3.862 | 8.579 | 17.309 | 100.90 |

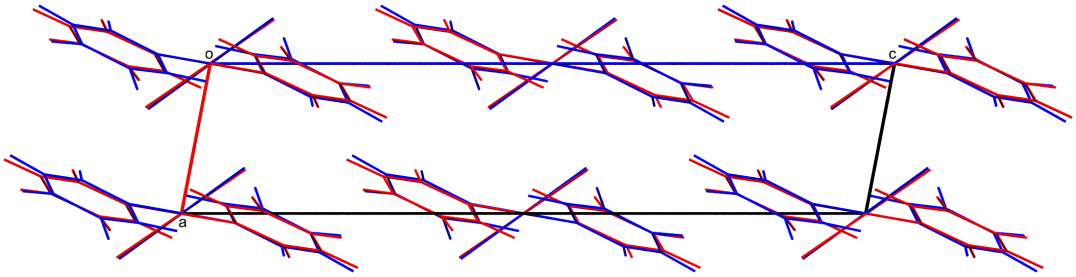


**Figure S5**
CuCP: overlay of the final structure from a user-controlled Rietveld refinement (red) and the published single crystal structure (after transformation from $P2_1/n$ to $P2_1/c$, blue). View along [010].

## S7. Pawley fits of DFQ, DCQ and DHDCQ

The unit cells resulting from the Rietveld refinements of DFQ (Fig. 5, Table S5, Table S17), DCQ (Fig. 6, Table 5, Table S17) and DCDHQ (model B1Z1, Fig. 9, Table 8) were compared to the Pawley fits for the same powder data. The cells dimensions of DFQ and DCQ from the Pawley fit (Table S16) are in good agreement with the Rietveld refinements of those structures and the corresponding difference curves (Fig. S6 and Fig. S7) are quite flat. The difference curve of the Pawley fit of DCDHQ (Fig. S8) is less smooth than those of DFQ or DCQ, and indicates that the sample may contain traces of other phases.

**Table S16**
Pawley fits of DFQ, DCQ and DCDHQ.

| Model | DFQ (B) | DCQ | DHDCQ (B1Z1) |
|---|---|---|---|
| Space group | $P2_1/c$ | $P\bar{1}$ | $P\bar{1}$ |
| $Z$ | 2 | 1 | 1 |
| $R_{exp}$ / % | 1.276 | 1.280 | 1.280 |
| $R_{wp}$ / % | 5.160 | 6.759 | 9.946 |
| $R_{wp}$' / % | 9.018 | 12.249 | 17.679 |
| *GoF* | 4.045 | 5.279 | 7.770 |
| $V/Z$ / Å$^3$/mol | 358.54 | 358.33 | 361.44 |
| $a$ / Å | 14.2113(12) | 3.7715(13) | 3.8492(71) |
| $b$ / Å | 3.76353(13) | 6.4745(20) | 6.7222(21) |
| $c$ / Å | 13.6958(18) | 15.7833(73) | 15.6764(41) |
| $\alpha$ / ° | 90 | 93.695(33) | 87.476(15) |
| $\beta$ / ° | 102.595(15) | 92.154(35) | 91.238(51) |
| $\gamma$ / ° | 90 | 100.814(51) | 74.742(53) |

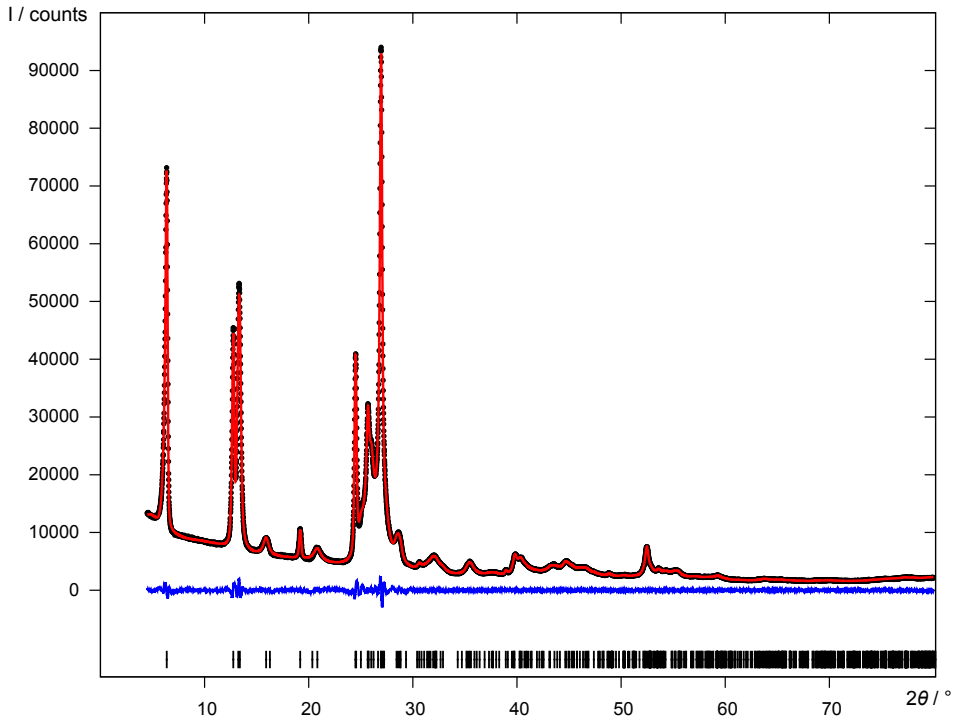


**Figure S6**
Pawley fit of DFQ ($P2_1$/c, Z=2, model B). Experimental X-ray powder diagram (black dots), simulated diagram of refined cell (red line), difference curve (blue line) and reflection positions (black bars).

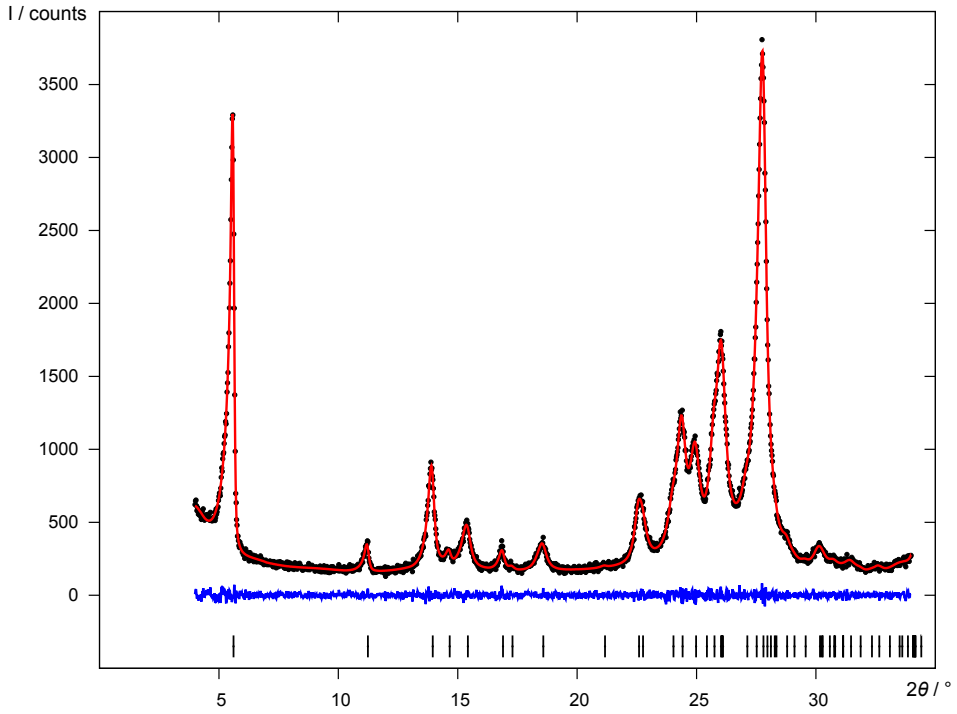


**Figure S7**
Pawley fit of DCQ ($P\bar{1}$, Z=1). Experimental X-ray powder diagram (black dots), simulated diagram of refined cell (red line), difference curve (blue line) and reflection positions (black bars).

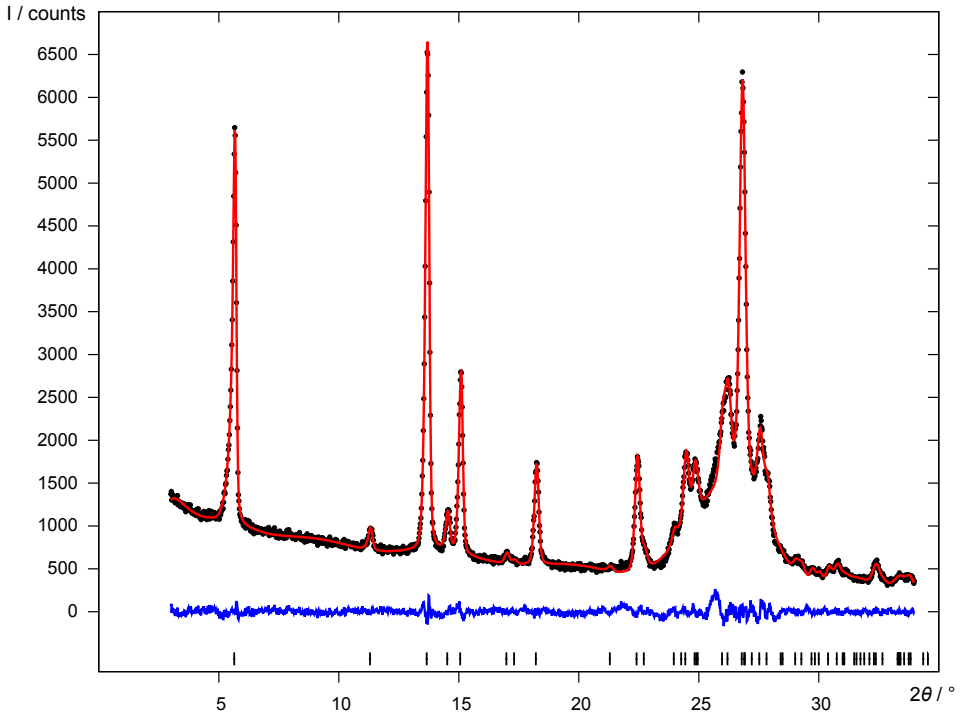


**Figure S8**
Pawley fit of DCDHQ ($P\bar{1}$, Z=1, model B1Z1). Experimental X-ray powder diagram (black dots), simulated diagram of refined cell (red line), difference curve (blue line) and reflection positions (black bars).

## S8. Experimental details of the crystal structure determinations of DFQ and DCQ

**Table S17**
Experimental details of the crystal structure determinations of DFQ and DCQ (CIF file in the supporting information)

| | DFQ | DCQ |
|---|---|---|
| Crystal data | | |
| Chemical formula | $C_{20}H_{10}F_2N_2O_2$ | $C_{20}H_{10}Cl_2N_2O_2$ |
| $M_r$ | 348.30 | 381.20 |
| Crystal system, space group | Monoclinic, $P2_1/c$ | Triclinic, $P\overline{1}$ |
| Temperature (K) | 300 | 300 |
| $a$, $b$, $c$ (Å) | 14.2169 (17), 3.7679 (2), 13.7214 (15) | 3.7718 (11), 6.4792 (18), 15.774 (5) |
| $\alpha$, $\beta$, $\gamma$ (°) | 90, 102.298 (14), 90 | 93.74 (3), 92.19 (2), 100.918 (19) |
| $V$ (Å$^3$) | 718.16 (13) | 377.20 (19) |
| $Z$ | 2 | 1 |
| Radiation type | Cu $K\alpha_1$, $\lambda$ = 1.54056 Å | Cu $K\alpha_1$, $\lambda$ = 1.54056 Å |
| Data collection | | |
| Diffractometer | STOE STADI-P | STOE STADI-P |
| Specimen mounting | Prepared between polymer films | Prepared between polymer films |
| Data collection mode | Transmission | Transmission |
| Scan method | Continuous | Continuous |
| $2\theta$ values (°) | $2\theta_{min}$=4.50 $2\theta_{max}$=79.99 $2\theta_{step}$=0.01 | $2\theta_{min}$=4.00 $2\theta_{max}$=33.98 $2\theta_{step}$=0.02 |
| Refinement | | |
| $R$ factors and goodness of fit | $R_p$=0.054, $R_{wp}$=0.065, $R_{exp}$=0.015, $R(F)$=0.026, $\chi^2$=19.378 | $R_p$=0.040, $R_{wp}$=0.052, $R_{exp}$=0.046, $R(F)$=0.191, $\chi^2$=1.288 |
| No. of data points | 7550 | 1500 |
| No. of parameters | 104 | 111 |
| No. of restraints | 61 | 61 |
| H-atom treatment | Only H-atom coordinates refined | Only H-atom coordinates refined |

Computer programs: *FIDEL-GO*, *WinX$^{POW}$* (STOE & Cie, 2006), *TOPAS Academic* (Coelho, 2009), *Mercury* (Macrae *et al.*, 2008).

## References


Cheary, R. W. & Coelho, A. A. (1998). *J. Appl. Cryst.* **31**, 851–861.

Coelho, A. A., (2009). *TOPAS-Academic*. Version 4.2. Coelho Software, Brisbane, Australia.

Huang, R., Wang, C., Wang, Y. & Zhang, H. (2018). *Advanced Materials*, **30**, 1800814.

Macrae, C. F., Bruno, I. J., Chisholm, J. A., Edgington, P. R., McCabe, P., Pidcock, E., Rodriguez-Monge, L., Taylor, R., Streek, J. v. d. & Wood, P. A. (2008). *J. Appl. Cryst*, **41**, 466–470.

Pawley, G. S. (1981). *J. Appl. Cryst.* **14**, 357–361.

Spek, A. L. (2009). *Acta Cryst.* D**65**, 148–155.

STOE & Cie, (2006). *WinXPOW Version 2.15*. STOE & Cie GmbH, Darmstadt, Germany.